Anisotropic magnetotransport in the layered antiferromagnet TaFe$_{1.25}$Te$_3$

Rajeswari Roy Chowdhury [1,*], Samik DuttaGupta [2,3], Chandan Patra,[1] Anshu Kataria,[1]
Shunsuke Fukami [2,3,4,5,6] and Ravi Prakash Singh [1,†]

[1]*Department of Physics, Indian Institute of Science Education and Research Bhopal,*
Bhopal Bypass Road, Bhauri, Madhya Pradesh 462066, India
[2]*Center for Science and Innovation in Spintronics, Tohoku University, 2-1-1 Katahira, Aoba-ku, Sendai 980-8577, Japan*
[3]*Laboratory for Nanoelectronics and Spintronics, Research Institute of Electrical Communication,*
Tohoku University, 2-1-1 Katahira, Aoba-ku, Sendai 980-8577, Japan
[4]*Center for Innovative Integrated Electronic Systems, Tohoku University, 468-1 Aramaki Aza Aoba, Aoba-ku, Sendai 980-0845, Japan*
[5]*WPI-Advanced Institute for Materials Research, Tohoku University, 2-1-1 Katahira, Aoba-ku, Sendai 980-8577, Japan*
[6]*Inamori Research Institute for Science, Shijo, Shimogyo-ku, Kyoto 600-8411, Japan*

The discovery of fascinating ways to control and manipulate antiferromagnetic materials have garnered considerable attention as an attractive platform to explore novel spintronic phenomena and functionalities. Layered antiferromagnets (AFMs) exhibiting interesting magnetic structures can serve as an attractive starting point to establish novel functionalities down to the two-dimensional limit. In this work, we explore the magnetoresistive properties of the spin-ladder AFM TaFe$_{1.25}$Te$_3$. Magnetization studies reveal an anisotropic magnetic behavior resulting in the stabilization of a spin-flop configuration for $H \perp$ (10-1) plane (i.e., out-of-plane direction). Angle-dependent longitudinal and transverse magnetoresistances show an unusual anharmonic behavior. A significant anisotropic enhancement of magnetoresistance when $H \perp$ (10-1) plane compared to $H \parallel$ (10-1) directions has been observed. The present results deepen our understanding of the magnetoresistive properties of low-dimensional layered AFMs, and point towards the possibility of utilizing these novel material systems for antiferromagnetic spintronics.

I. INTRODUCTION

The capability to manipulate and control antiferromagnets (AFMs) via electrical techniques has provided unprecedented opportunities for the development of materials, and new-concept electronic devices with different functionalities [1–3]. Previous works utilizing AFMs in quasi-three-dimensional heterostructure geometry have demonstrated promising characteristics such as electrical control of antiferromagnetic Néel vector and stabilization of AFM skyrmions [4–7], expected to pave the way for future AFM-based memories and devices for unconventional computing architectures. On the other hand, there has not been much focus on low-dimensional (layered and chainlike) AFMs, fundamentally and technologically interesting due to their abilities to introduce new functionalities and translate the existing properties down to the two-dimensional (2D) limit. Among the different families of layered AFMs, Fe-based chalcogenides are attractive owing to their reasonably high magnetic ordering temperature (T_N), coexistence, and competing relationships between superconductivity and magnetism [8–12]. Among them, layered TaFe$_{1+x}$Te$_3$ is interesting [13,14], where the Fe atoms form a two-leg ladder along the principal axis (i.e., b axis)

but with a zigzag shape representing an intriguing quasi-one-dimensional magnetic system. TaFe$_{1+x}$Te$_3$ crystallizes in a monoclinic structure, consisting of Ta-Fe bonded layers sandwiched between the Te layers [Fig. 1(a)]. There are also excess Fe atoms, randomly occupying some interstitial sites, potentially influencing the magnetic order in the Fe-Te layers [15,16]. Previous magnetic and magnetoresistance measurements on TaFe$_{1.21}$Te$_3$ suggest a spin-density wave magnetic character, below T_N, where the neighboring spins within each ladder are antiparallelly coupled [17]. On the other hand, neutron diffraction measurements on TaFe$_{1.25}$Te$_3$ indicate a ferromagnetic two-leg zigzag ladder configuration which is antiferromagnetically coupled to its neighboring layers [18]. Despite these studies, a detailed investigation concerning the magnetoresistive responses originating from the unique ladderlike magnetic structure and its modification with varying number of layers remains unexplored. Owing to the layer dependent magnetic character, TaFe$_{1+x}$Te$_3$ serves as an archetype system for understanding the impact of dimensionality on magnetic order, electronic, topological, and correlated physics, crucial for future development of novel layered materials. Furthermore, despite its low T_N, TaFe$_{1.25}$Te$_3$ is an interesting candidate for exploring the physics of intralayer and interlayer exchange interactions, and electrical current-induced effects in few-monolayer heterostructures which could be crucial for future development for layered material-based devices. The interplay of

*rajeswari@iiserb.ac.in
†rpsingh@iiserb.ac.in
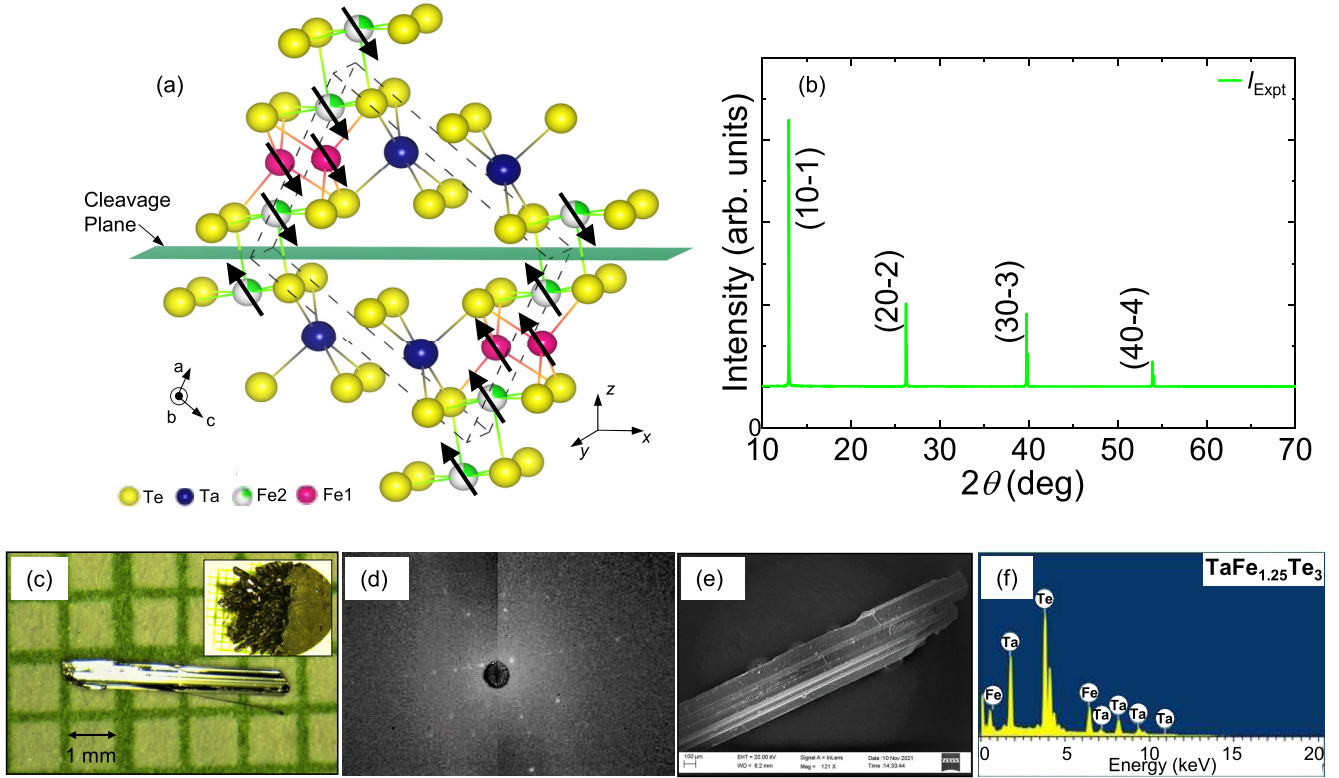
FIG. 1. (a) Crystal structure of $TaFe_{1+x}Te_3$. The interstitial Fe atoms are denoted by white-green circles. (b) Out-of-plane x-ray diffraction pattern of $TaFe_{1.25}Te_3$ single-crystalline sample at room temperature. (c) Optical micrograph of $TaFe_{1.25}Te_3$ single crystal utilized in this study. Inset shows the needlelike single crystals obtained by chemical vapor transport synthesis. (d) Laue diffraction pattern of the single crystal. (e) Scanning electron micrograph image of the needlelike nature of $TaFe_{1.25}Te_3$ single crystal. (f) Energy dispersive x-ray analysis (EDX) spectra for $TaFe_{1.25}Te_3$.

this unique AFM order and its preferential alignment with respect to certain crystallographic directions can manifest in anisotropic magnetoresistive behavior, providing qualitative information concerning magnetic anisotropy, a key parameter concerning the potential of a material system for development of spintronic devices. Intuitively, the application of magnetic field (H) on this A-type interlayer antiferromagnetic coupling could also be interesting, where a potential transformation of the relatively weak AFM interaction into an Ising-like or XY-type ferromagnet (FM) state [19–22] can consequently result in a significant magnetoresistance (MR). While such an alteration of AFM order by H is generally deemed to be difficult, a strong coupling between the spin and lattice degrees of freedom can result in a modification of electronic structure through a spin-flop transition, manifesting in significant MR. In addition, MR, and its angular dependence in naturally occurring layered compounds can also serve as an alternative route for understanding of the exotic magnetic structure. Finally, the existence of such a unique MR effect is expected to introduce different avenues for utilization of AFMs.

In this work, we have explored the magnetic, temperature, and angle-dependent MR effects in layered AFM $TaFe_{1+x}Te_3$. Temperature dependent magnetization (M) measurements show antiferromagnetic ordering at ≈ 200 K, consistent with previous study [17]. An applied magnetic field (H) perpendicular to the (10-1) plane shows the existence of a spin-flop

transition at $T \approx 130$ K, associated with an increase of M and an abrupt drop of the longitudinal MR, only for $H\perp$ (10-1) plane. Interestingly, the spin-flop transition also results in a sharp deviation of the angle-dependent longitudinal MR behavior from its usual harmonic nature, manifesting in a strong anharmonicity in angular dependence. Along with this, there is a significant enhancement of longitudinal MR, compared to $H||$ (10-1) configuration. Our work deepens the understanding of MR properties in layered AFMs and indicates the possibility of utilizing this magnetoresistive effect as a prospective scheme for introducing spintronic functionalities in layered AFMs.

II. EXPERIMENTAL DETAILS

Single crystals of $TaFe_{1.25}Te_3$ (TFT, hereafter) were grown by the chemical vapor transport (CVT) method. A stoichiometric mixture of Ta (3N), Fe (3N), and Te (3N) was ground thoroughly and sealed in an evacuated quartz tube along with $TeCl_4$ as the transport agent. The tube was kept in a two-zone furnace at a temperature gradient of $690\,°C/660\,°C$. Needle shaped crystals were obtained after ten days. Structural analysis of the crystals was performed by x-ray diffraction (XRD) at room temperature using a PANalytical diffractometer with Cu-K_α radiation. Magnetic properties were characterized using a superconducting quantum interference device (SQUID) in the temperature range 5–300 K. From the synthesized

single crystals, several mm-sized samples were selected and cut into square/rectangular shapes of typical sizes of $\sim$ 1–4 × 1–4 mm². The surface of these samples was freshly cleaved in an inert atmosphere. Current and voltage electrodes were fabricated *in situ* by connecting Au wires on the samples by silver epoxy. Electrical and magnetotransport measurements were performed by a physical property measurement system using a conventional four-probe technique under an applied dc I [$\parallel$ (10-1) plane] of magnitude 10 mA. Longitudinal (ρ_L) and transverse (ρ_T) resistivities were obtained as a function of temperature (T) and applied magnetic field (H).

III. RESULTS AND DISCUSSIONS

In this section, we show the experimental results and discuss the magnetic and magnetotransport properties of TFT single crystals.

A. Structural characterization of TaFe$_{1.25}$Te$_3$ (TFT)

Figure 1(a) shows the crystal structure of TFT. The layered ternary compound crystallizes in a monoclinic structure (space group $P2_1/m$), comprising layers of Ta-Fe sandwiched between Te layers, forming TaFeTe$_3$. The excess Fe (atomic percentage 0.25) is expected to partially occupy the interstitial sites in a random manner [shown as white-green spheres in Fig. 1(a)]. Figure 1(b) shows the experimental results of out-of-plane XRD for TFT single crystals. The observed Bragg peaks can be indexed with ($l0$-l) peaks, perpendicular to the sample surface. Besides, any additional peak corresponding to unreacted elements or due to unintentional formation of other Ta-Fe-Te variants was not observed. Rietveld refinement of the XRD data of a powdered sample (see Appendix) yields lattice parameters to be $a = 7.422$ Å, $b = 3.640$ Å, $c = 10.001$ Å, and $\beta = 109.144°$ respectively, consistent with the earlier reports [13,14]. Figure 1(c) shows the optical microscope image of needlelike single crystals of TFT. The inset shows the collection of as-grown crystals. Figure 1(d) shows the Laue diffraction pattern confirming formation of good quality of the obtained crystals. A scanning electron microscope (SEM) image of a needlelike layered crystal is shown in Fig. 1(e). The chemical composition of the grown crystals was confirmed from atomic percentage ratios obtained from energy-dispersive X-ray (EDX) spectroscopy measurements [Fig. 1(f)] within the instrumental limit.

B. Magnetic and magnetocaloric properties of TFT

Figures 2(a) and 2(b) show the experimental results of temperature (T) dependence of field-cooled (FC) magnetic susceptibility (χ) under different magnetic field $\mu_0H = 0.1$, 1, 5, 7 T, applied parallel or perpendicular to the (10-1) sample plane (i.e., in plane or out of plane with respect to crystal), respectively. Magnetic susceptibility (χ) under applied $\mu_0H = 0.1$ T parallel or perpendicular to the (10-1) plane shows a sharp transition at $T \approx 194$ K, demonstrating the onset of antiferromagnetic order. The observed Néel temperature (T_N) is slightly higher than previous reports on single crystals [17,18], but almost matches that of polycrystalline TaFe$_{1.25}$Te$_3$ ($T_N \approx 200$ K) [13]. When $H \perp$ (10-1) plane (i.e., along the out-of-plane direction), T_N is weakly suppressed
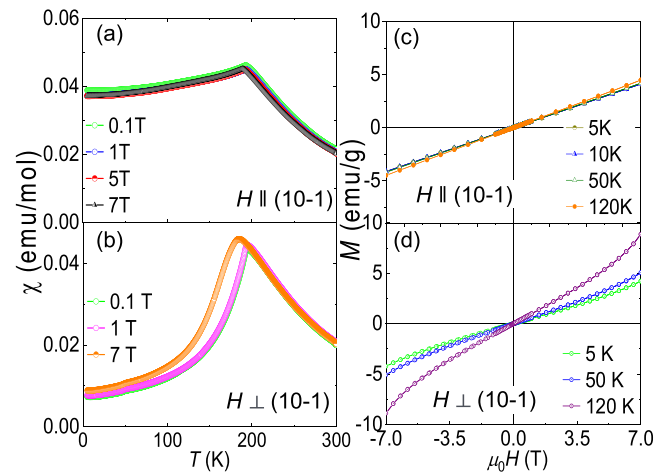
FIG. 2. (a) Magnetic susceptibility (χ) versus temperature (T) under various magnetic fields $\mu_0H = 0.1$, 1, 5, and 7 T applied parallel to (10-1) plane, i.e., along the plane of the crystal. (b) χ versus T under various magnetic fields $\mu_0H = 0.1$, 1, and 7 T applied perpendicular to (10-1) plane, i.e., along the out-of-plane direction. (c) Field (H) dependence of magnetization (M) for TaFe$_{1.25}$Te$_3$ single crystal at $T = 5$, 10, 50, and 120 K, for applied H parallel to (10-1) plane. (d) Experimental results for M versus H at $T = 5$, 50, and 120 K, for applied H perpendicular to (10-1) plane.

from $\approx$194 K for $\mu_0H = 0.1$ T to $\approx$183 K for $\mu_0H = 7$ T. Along with the reduction of T_N, some previous results also reported a ferromagneticlike nature within a small temperature range below T_N, attributed to the alignment of excess Fe atoms towards the applied H direction [23]. The coupling of this glasslike ferromagnetic state to the bulk AFM order was shown to result in a considerable exchange bias field of $\approx$0.16 T below 10 K [22]. Figures 2(c) and 2(d) show the results of magnetization (M)-H measurements for applied H along the (10-1) or $\perp$ (10-1) plane, respectively. For $5 < T < 50$ K, M increases linearly with H, representative of the antiferromagnetic nature of the system. At higher T ($\geqslant 120$ K), for applied $H \perp$ (10-1) plane, we observe an increasing tendency above a threshold field, reminiscent of the flopping of the antiferromagnetic moments leading to an enhancement of M. On the other hand, for $H \perp$ (10-1) plane, we do not observe such behavior up to maximum applied $\mu_0H = 7$ T. Unlike the previous report [23], we also do not observe any hysteretic feature in M-H, indicating a virtually nonexistent spin-glass-like state. Besides, we observe a considerable difference in magnitude of χ for applied $H \parallel$ (10-1) or $\square$ (10-1) plane, clearly indicating the existence of an antiferromagnetic anisotropy in the system.

To further characterize the anisotropic magnetic properties of TFT, isothermal magnetic entropy change (ΔS_M) was calculated, under applied $H \parallel$ (10-1) and $\perp$ (10-1) plane directions within a T range 160–250 K from magnetization isotherms. ΔS_M was obtained from M-H curves using Maxwell's relation [24,25],

$$\Delta S_M(T, H) = \int_0^H \left[\frac{\partial S(T, H)}{\partial H} \right]_T dH \quad (1)$$
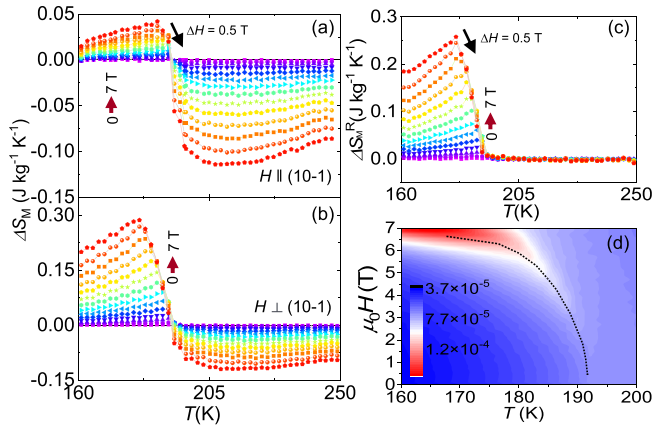
FIG. 3. (a) Temperature (T) dependence of magnetic entropy change (ΔS_M) under application of magnetic fields $\mu_0 H = 1–7$ T applied perpendicular to (10-1) plane. (b) Experimental results of similar measurements under application of magnetic fields $\mu_0 H = 1–7$ T applied parallel to (10-1) plane. (c) T dependence of rotational magnetic entropy change (ΔS_M^R), defined as the difference between ΔS_M from (a) and (b) at a constant T and H. (d) T dependence of spin-flop field, obtained from M-H measurements under applied $H \perp$ (10-1) plane. Color bar in (d) indicates the magnitude of the first derivative of magnetization (from M-H measurements).

$$= \int_0^H \left[\frac{\partial M(T,H)}{\partial T} \right]_H dH. \quad (2)$$

Figures 3(a) and 3(b) show the T dependence of ΔS_M under $\mu_0 H = 1–7$ T, applied ∥ or ⊥ (10-1) plane, respectively. As we decrease T from 250 K, ΔS_M is initially negative when the system is in the paramagnetic state. Around $T \approx 194$ K, ΔS_M changes sign owing to the onset of AFM order, coinciding with T_N obtained from magnetization measurements. Subsequently, the application of H in the antiferromagnetic state results in adiabatic cooling owing to the enhancement of configurational entropy of the spin structure, and reduction of the lattice entropy. Interestingly, under $\mu_0 H = 7$ T, applied ⊥ (10-1) plane, $\Delta S_M = 0.29$ J/kg K, which is significantly larger than that for applied H∥ (10-1) plane of identical magnitude ($\Delta S_M = 0.04$ J/kg K). We also calculate the rotational magnetic entropy change (ΔS_M^R) as

$$\Delta S_M^R(T,H) = \Delta S_M(T, H_{\perp(10-1)}) - \Delta S_M(T, H_{\parallel(10-1)}). \quad (3)$$

Figure 3(c) shows the T dependence of ΔS_M^R under applied $\mu_0 H = 1–7$ T, confirming the anisotropic magnetic character of the system. The sign of ΔS_M^R [defined as Eq. (3)] is always positive, considered to be indirect evidence of strong AFM coupling among the Fe moments, perpendicular to the (10-1) plane. The magnitude of $\Delta S_M^R \approx 0.25$ J/kg K, for TFT, is comparable to van der Waals ferromagnetic Fe_3GeTe_2 [26]. Furthermore, we have observed that an increase of H results in a shift of the peak position towards lower T. The observed feature is most likely due to the flopping of the antiferromagnetic moments under applied H which can be confirmed from Fig. 3(d), and, as shown later, plays a crucial role in governing
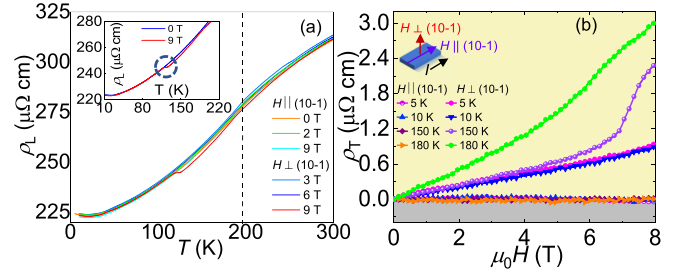
FIG. 4. (a) Temperature (T) dependence of longitudinal resistivity (ρ_L) under various magnetic field (H), applied parallel or perpendicular to (10-1) plane. Inset in (a) shows ρ_L vs T under $\mu_0 H = 9$ T is applied ⊥ (10-1) plane. Broken line indicates the T at which there is a nonmonotonic variation in ρ_L. (b) Applied H dependence of transverse resistivity (ρ_T) at various T. Inset in (b) shows the direction of the applied H and current (I) for ρ_L and ρ_T measurements.

the unique magnetotransport features of this layered AFM system.

C. Magnetotransport properties of $TaFe_{1.25}Te_3$ (TFT)

Figure 4(a) shows the T dependence of longitudinal resistivity (ρ_L) under applied dc I [∥ (10-1) plane] i.e., along the crystal plane [inset of Fig. 4(b) shows the schematics of the measurement setup]. We observe a metallic behavior over the entire range with or without applied H and a transition at $T \approx 195$ K, approximately around the Néel temperature, determined from magnetization measurement. When $\mu_0 H = 9$ T is applied ⊥ (10-1) plane, we also observe an anomalous transition at $T \approx 120$ K [inset of Fig. 4(a)], in agreement with the M-H measurements [Fig. 2(d)]. Figure 4(b) shows the H dependence of transverse resistivity (ρ_T) at various T. Furthermore, we also observe a resistivity upturn for $T \leqslant 30$ K, possibly associated with the emergence of interplanar electronic transport mediated by interstitial Fe [Fe(2)] atoms, in addition to that within the Ta-Fe network [18]. Below $T \approx 150$ K, ρ_T increases linearly under H, applied either ∥ or ⊥ (10-1) plane. Above this threshold, for $H \perp$ (10-1) plane, two distinct regimes are evident, *viz.*, a linear regime followed by a sudden rise in ρ_T, tentatively attributed to arise from the net magnetization acquired by the flopping of the AFM moments. Carrier concentration calculated using the linear part of the field dependence of transverse resistivity below the spin-flop field yields a carrier density $n \approx 0.99 \times 10^{21}$ cm^{-3} at 150 K. To investigate the origin for the observed features, we measure the H dependence of ρ_L at various T, and calculate magnetoresistance (MR) (in %) = $[\rho_L(H) - \rho_L(0)]/\rho_L(0)$ [Fig. 5(a)]. At low temperatures ($10 \leqslant T \leqslant 100$ K), for both H∥ or ⊥ (10-1) plane, MR exhibits a small negative amplitude ($\leqslant 0.5$%). However, an increase in T ($\geqslant 130$ K), for $H \perp$ (10-1) plane, results in a slightly positive MR succeeded by a sharp drop. The threshold H corresponding to this drop decreases from ≈ 8.4 T at $T = 130$ K, to ≈ 6.4 T at $T = 180$ K. Interestingly, no such behavior is observed for applied H∥ (10-1) plane [Fig. 5(b)]. To understand the factors responsible towards this distinct behavior, it is necessary to consider the impact of
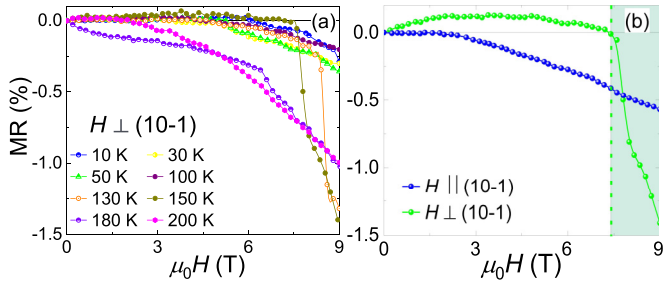
FIG. 5. (a) Temperature (T) dependence of magnetoresistance (MR) (in %) versus applied magnetic field (H), applied perpendicular to (10-1) plane (i.e., H|| out-of-plane direction). (b) Comparison of MR for applied H|| (10-1) or $\perp$ (10-1) plane directions, at T = 150 K. Dotted arrow in (b) indicates the observed magnitude of H at which the sharp drop in ρ occurs, at T = 150 K.

applied H on the bulk antiferromagnetic order of TFT. TFT possesses a zigzag ladder configuration of Fe moments and additional interstitial Fe moments, running parallel to the b axis [15–18,27]. However, they mainly differ on the magnetic

arrangement of Fe moments within each zigzag ladder and their coupling to the subsequent layers.

Some previous studies indicated an intraladder antiferromagnetic arrangement of neighboring moments and spin-density wave type AFM structure [17], while neutron diffraction and angle-resolved photoemission spectroscopy measurements [18,27] indicate an intraladder ferromagnetic alignment of the Fe moments with an antiferromagnetic coupling between consecutive ones (A-type AFM order). Furthermore, this AFM ground state is also composed of a quasi-two-dimensional Fermi surface with sizeable interladder hopping mediated by superexchange interaction [27]. The Fe moments within a ladder are arranged ferromagnetically at an angle of 17.6° with respect to the (10-1) direction (i.e., the conventional out-of-plane direction) and are antiferromagnetically coupled to the nearest neighboring chains. Considering this A-type AFM ground state, the sharp drop in longitudinal MR for $H\perp$ (10-1) plane [Fig. 5(a)] might be attributed to arise from an interladder spin-flop configuration and/or spin-flop followed by rotation of the AFM moments perpendicular to the applied H. The absence of a similar
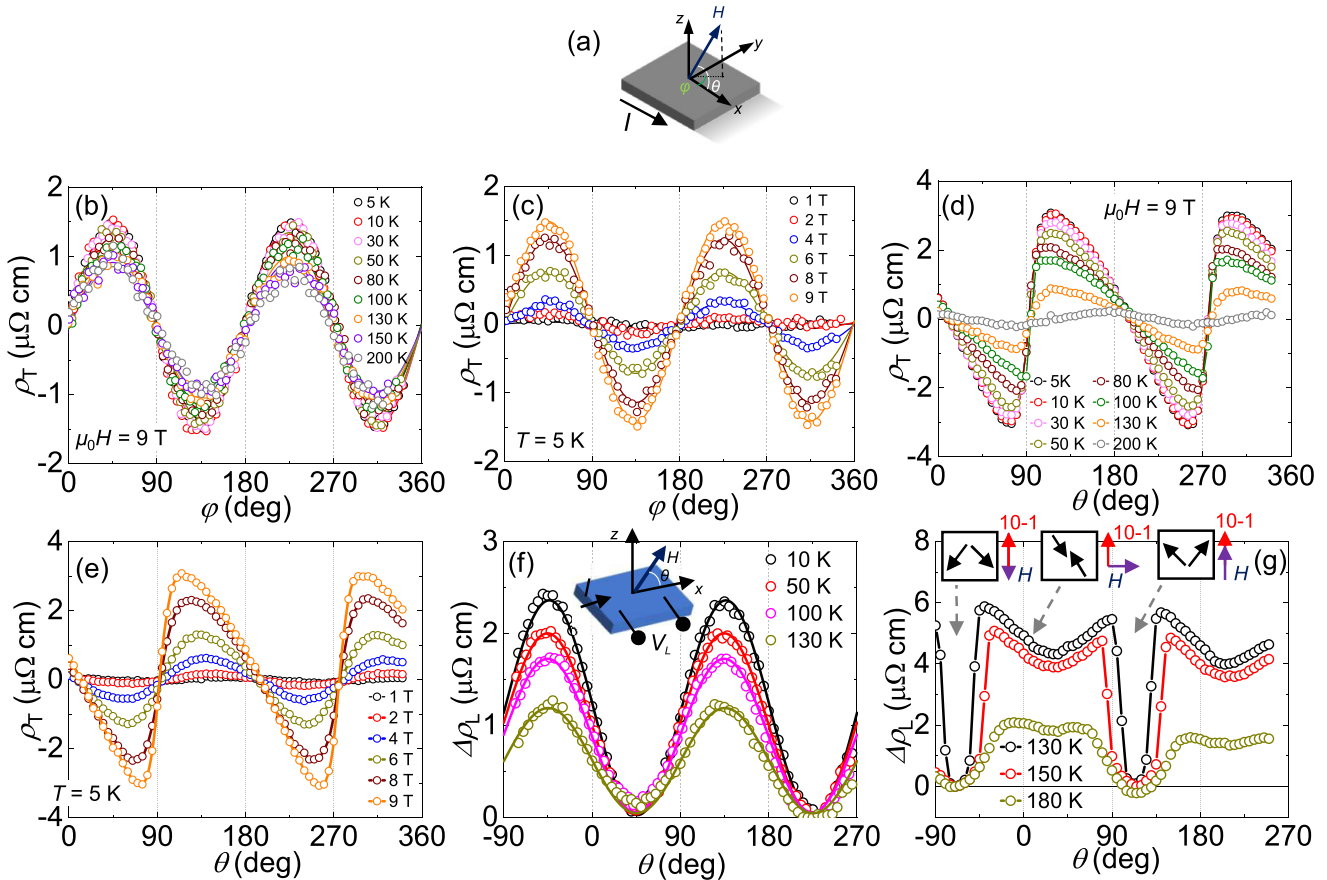
FIG. 6. (a) Schematic representation of the measurement configuration utilized in this work. The azimuthal (θ) and polar (φ) angles are defined as the angle subtended by the applied magnetic field (H) with respect to the applied current (I) along x direction. (b) φ dependence of transverse resistivity (ρ_T) under constant magnetic field $\mu_0 H$ = 9 T [H|| (10-1) plane], at various temperatures (T). (c) φ dependence of ρ_T under varying magnitudes of H at T = 5 K. (d) θ dependence of ρ_T under constant magnetic field $\mu_0 H$ = 9 T [$H\perp$ (10-1) plane], at various T. (e) θ dependence of ρ_T under varying magnitudes of H, at T = 5 K. (f) θ dependence of longitudinal resistivity (ρ_L) under constant magnetic field $\mu_0 H$ = 6 T at various T (10 $\leqslant T \leqslant$ 130 K). (g) Experimental results of similar measurements under $\mu_0 H$ = 8 T, for $T \geqslant$ 130 K. Solid lines in (b), (c), and (f) denote the fitting of the experimental data with the harmonic sine squared dependence. Schematic diagrams in (g) represent possible spin configurations in the spin-flop and AFM configurations.

sharp drop in longitudinal MR for $H || $ (10-1) plane [Fig. 5(b)] indicates the existence of an anisotropic behavior, restricting the stabilization of the spin-flop configuration only for certain directions of applied H. Transverse resistivity (ρ_T) measurements also support a similar scenario [Fig. 4(b)], where the sudden rise in ρ_T for $T \geqslant 150$ K can be attributed to arise from the net magnetization acquired by the spin-flopped configuration, for applied $H || $ (10-1) plane. As shown below, the stabilization of a unique AFM ground state and the realization of an anisotropic spin-flop configuration renders drastic ramifications into the angular magnetoresistive properties of TFT.

To clarify the manifestations of the anisotropic magnetotransport behavior, we measured the angle dependent longitudinal and transverse magnetoresistance at various T. Figure 6(a) shows the schematic diagram of the measurement geometry, and the definitions of the azimuthal (angle φ between H and I) and polar (angle θ between H and I) angles with respect to the single crystal. An applied dc I ($||$ (10-1) plane) was passed through the single crystal along the x direction (i.e., along the crystal plane). The resulting change in longitudinal or transverse voltages were measured under rotation of external H of constant magnitude along the azimuthal and polar planes. Intuitively, θ sweep corresponds to H rotating from a magnetic hard ($\theta \approx 0°$) to easy ($\theta \approx 72.4°$) direction, compared to φ sweep, enabling us to quantitatively clarify its impact on the magnetoresistive features. Figures 6(b) and 6(c) show experimental results of ρ_H versus φ, under constant H ($T = 5$ K) and T ($\mu_0 H = 9$ T), respectively. We observe that ρ_H versus φ follows a twofold symmetry with a $\sin^2 \varphi$ behavior [solid lines in Figs. 6(b) and 6(c)]. Furthermore, the amplitude of the $\sin^2 \varphi$ dependence monotonically decreases with increasing T or decreasing H. Owing to the A-type AFM order along with the absence of spin-flop configuration for $H || $ (10-1) plane, the observed magnetoresistive behavior can be interpreted as anisotropic magnetoresistance (AMR), arising from the orientation of the antiferromagnetic Néel vector with respect to I, commonly found in most FM or AFMs. On the other hand, significant deviations from the conventional AMR [28,29] were observed for H rotations along θ [Figs. 6(d) and 6(e)]. ρ_T versus θ curves deviate significantly from the harmonic behavior and show a sharp sign reversal as $H \perp$ (10-1) plane. Interestingly, the anharmonic behavior is strongly dependent on H [Fig. 6(e)], and weakly varies with T [Fig. 6(d)]. This indicates that the underlying origin of this anharmonic behavior might not be dominantly linked to the flopping of the AFM moments, induced by the applied H. While we cannot rule out any contribution from spin-flop configurations, we speculate that the anharmonic nature might be strongly influenced by the magnetic anisotropy of TFT, preferring an AFM alignment perpendicular to the (10-1) planes. To further explore the peculiar nature of the magnetotransport features of TFT, we also study the effect of H rotation (θ) on ρ_L [Figs. 6(f) and 6(g)]. For applied H less than the spin-flop field ($10 \leqslant T \leqslant 130$ K, $\mu_0 H = 6$ T), the MR curves show a harmonic behavior ($\sin^2 \theta$ dependence). Interestingly, as H is larger than the spin-flop field ($T \geqslant 130$ K, $\mu_0 H = 8$ T) we observe a significantly different behavior, strongly anharmonic in nature with the appearance of plateaulike features for certain θ, along with
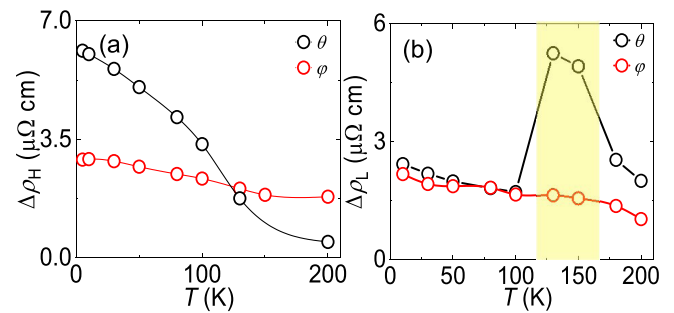
FIG. 7. (a) Temperature (T) dependence of the amplitude of transverse resistivity (ρ_T) for H rotations along azimuthal (θ) and polar (φ) directions under applied $\mu_0 H = 8$ T. (b) T dependence of the amplitude of longitudinal resistivity (ρ_L) for H rotations along azimuthal (θ) and polar (φ) directions under applied $\mu_0 H = 8$ T.

a significant increase in the magnitude of ρ_L. Furthermore, an increase in T, in this regime at fixed $\mu_0 H = 8$ T, also results in a reduction of ρ_L magnitude, attributed to an enhancement of spin fluctuation near T_N.

In AFM systems, the spin-flop transition refers to a situation where there is a transition from an AFM order to a noncollinear spin configuration or a canting of the magnetic moments, both of which result in a finite magnetic moment. A reversible transition from an AFM order to a spin-flop state might be useful for applications either by utilizing the anomalous Hall effect or associated changes in the linear magnetoresistance due to strong spin-lattice couplings [19–22, 28–31]. However, the utilization of the spin-flop effect is overly complicated due to at least two reasons: (i) requirement of uniaxial anisotropy and an external field, and (ii) typical transition spin-flop fields are several tens of T, which is too high for real applications [32–34]. From this perspective, a layered AFM system can be reminiscent of a synthetic AFM or ferrimagnetic systems, where the spin flop field is proportional to the difference of sublattice magnetizations. To get a deeper understanding of the underlying physics governing the different magnetoresistive behaviors, we have extracted the magnitude of the observed magnetoresistances versus θ and φ [Figs. 7(a) and 7(b)]. For either θ or φ rotations, the amplitude of the transverse resistivity ($\Delta \rho_T$)) monotonically decreases with increasing T, as expected for a MR signal originating from magnetic order. On the other hand, the amplitude of longitudinal resistivity ($\Delta \rho_L$) shows a dramatic behavior. Starting from $T = 10$ K, for θ or φ rotations, $\Delta \rho_L$ slightly decreases up to 100 K thereafter, showing a significant enhancement in the T range 130–150 K (for θ rotation), while it decreases monotonically for φ rotations. Considering an A-type AFM ground state of TFT with an intralayer ferromagnetic alignment, for φ rotation, the H is always perpendicular to the Néel vector, roughly oriented at $\approx 18°$ with respect to the surface normal. We speculate that no further discernable reorientation of the Néel vector occurs under φ rotation resulting in a monotonic decrease of MR behavior. As stated before, θ rotation results in the H rotating between magnetically easy and hard directions which can have a profound effect on the interlayer AFM moments. Interestingly, the observed sharp drop in ρ_L occurs when H is perpendicular to the (10-1) plane, i.e., applied almost along the magnetically easy directions. As
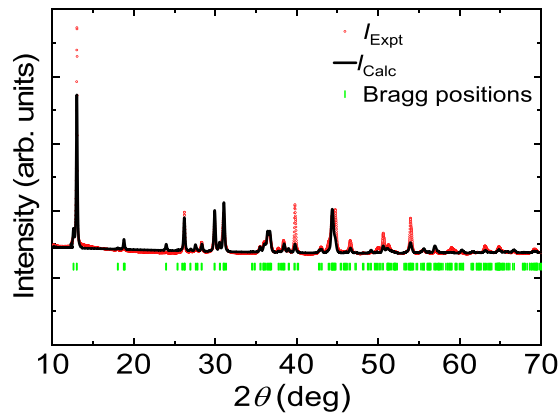
FIG. 8. Experimental results of x-ray diffraction for $TaFe_{1.25}Te_3$ polycrystalline sample in theta (θ)-2θ geometry.

a result, the significant enhancement in $\Delta\rho_L$ is tentatively attributed to the stabilization of a spin-flop configuration of the interlayer AFM configuration. Our results are also indicative of a strong interlayer magnetic coupling and represents an intriguing situation despite the large separation between the Fe moments between the adjacent layers. In a typical AFM, the magnitude of AMR originating either from the spin-orbit coupling of the electronic band structure or exchange coupling to an adjacent FM is small, roughly 0.5–1% [35,36]. On the other hand, the MR effect in the spin-flop configuration is substantially large, $\approx$3–4%. We believe that this work would open an unexplored pathway to utilize spin-flop configurations for introducing unique functionalities in antiferromagnetic spintronics.

IV. CONCLUSIONS

In conclusion, we have investigated the magnetic, temperature, and angle dependent longitudinal and transverse magnetoresistive effects in the layered AFM $TaFe_{1.25}Te_3$. Temperature and applied magnetic field dependent magnetization measurements reveal the existence of an anisotropic behavior, $H\perp$ (10-1) plane results in a spin-flop-like transition around $T \geqslant 130\,\mathrm{K}$ as opposed to an antiferromagnetic

nature for $H\perp$ (10-1) plane. The spin-flop behavior also manifests in anisotropic magnetotransport behavior and results in a sharp drop of linear resistivity at similar T and H configurations. Interestingly, the angle dependent longitudinal magnetoresistance around the spin-flop transition shows a strong anharmonic behavior along with a pronounced enhancement in its magnitude. A thorough investigation of magnetoresistive properties and observation of an unusual longitudinal MR around the spin-flop transition in a layered AFM system was unexplored. We believe that our results will inspire future experimental investigations with the variation of number of layers which might initiate a new paradigm of AFM spintronics with layered material systems. The present experimental results provide considerable insights into the remarkable magnetic and magnetotransport feature of layered AFMs, and suggest an alternative scheme to introduce novel spintronic functionalities in layered AFMs.

APPENDIX: X-RAY DIFFRACTION OF $TaFe_{1.25}Te_3$

To determine the lattice parameters of our sample, the single-crystalline samples were grounded for several hours and out-of-plane x-ray diffraction were performed. Figure 8 shows the XRD pattern of crushed single crystals of TFT at room temperature. Rietveld refinement of the XRD patterns using FULLPROF software yielded the lattice parameters reported in the main text, consistent with earlier reports [13] and the ICSD database.

[1] V. Baltz, A. Manchon, M. Tsoi, T. Moriyama, T. Ono, and Y. Tserkovnyak, Rev. Mod. Phys. **90**, 015005 (2018).

[2] T. Jungwirth, X. Marti, P. Wadley, and J. Wunderlich, Nat. Nanotechnol. **11**, 231 (2016).

[3] J. Železný, P. Wadley, K. Olejník, A. Hoffmann, and H. Ohno, Nat. Phys. **14**, 220 (2018).

[4] P. Wadley, B. Howells, J. Železný, C. Andrews, V. Hills, R. P. Campion, V. Novák, K. Olejník, F. Maccherozzi, S. S. Dhesi, S. Y. Martin, T. Wagner, J. Wunderlich, F. Freimuth, Y. Mokrousov, J. Kuneš, J. S. Chauhan, M. J. Grzybowski, A. W. Rushforth, K. W. Edmonds, B. L. Gallagher, and T. Jungwirth, Science **351**, 587 (2016).

[5] S. Y. Bodnar, L. Šmejkal, I. Turek, O. Gomonay, J. Sinova, A. A. Sapozhnik, H.-J. Elmers, M. Kläui, and M. Jourdan, Nat. Commun. **9**, 348 (2018).

[6] S. DuttaGupta, A. Kurenkov, O. A. Tretiakov, G. Krishnaswamy, G. Sala, V. Krizakova, F. Machherozzi, S. S. Dhesi, P. Gambardella, S. Fukami, and H. Ohno, Nat. Commun. **11**, 5715 (2020).

[7] W. Legrand, D. Maccariello, F. Ajejas, S. Collin, A. Vecchiola, K. Bouzehouane, N. Reyren, V. Cros, and A. Fert, Nat. Mater. **19**, 34 (2020).

[8] F. C. Hsu, J. Y. Luo, K. W. Yeh, T. K. Chen, T. W. Huang, P. M. Wu, Y. C. Lee, Y. L. Huang, Y. Y. Chu, D. C. Yan, and M. K. Wu, Proc. Natl. Acad. Sci. USA **105**, 14262 (2008).

[9] K. W. Yeh, T. W. Huang, Y. L. Huang, T. K. Chen, F. C. Hsu, P. M. Wu, Y. C. Lee, Y. Y. Chu, C. L. Chen, J. Y. Luo, D. C. Yan, and M. K. Wu, Europhys. Lett. **84**, 37002 (2008).

[10] M. H. Fang, H. M. Pham, B. Qian, T. J. Liu, E. K. Vehstedt, Y. Liu, L. Spinu, and Z. Q. Mao, Phys. Rev. B **78**, 224503 (2008).

[11] M. Bendele, A. Amato, K. Conder, M. Elender, H. Keller, H. H. Klauss, H. Luetkens, E. Pomjakushina, A. Raselli, and R. Khasanov, Phys. Rev. Lett. **104**, 087003 (2010).

[12] S. Margadonna, Y. Takabayashi, Y. Ohishi, Y. Mizuguchi, Y. Takano, T. Kagayama, T. Nakagawa, M. Takata, and K. Prassides, Phys. Rev. B **80**, 064506 (2009).

[13] M. E. Badding, J. Li, F. J. DiSalvo, W. Zhou, and P. P. Edwards, J. Solid State Chem. **100**, 313 (1992).

[14] C. Pérez Vicente, M. Womes, J. C. Jumas, L. Sánchez, and J. L. Tirado, J. Phys. Chem. B **102**, 8712 (1998).

[15] S. Li, C. de la Cruz, Q. Huang, Y. Chen, J. W. Lynn, J. Hu, Y.-L. Huang, F.-C. Hsu, K.-W. Yeh, M.-K. Wu, and P. Dai, Phys. Rev. B **79**, 054503 (2009).

[16] L. Zhang, D. J. Singh, and M. H. Du, Phys. Rev. B **79**, 012506 (2009).

[17] R. H. Liu, M. Zhang, P. Cheng, Y. J. Yan, Z. J. Xiang, J. J. Ying, X. F. Wang, A. F. Wang, G. J. Ye, X. G. Luo, and X. H. Chen, Phys. Rev. B **84**, 184432 (2011).

[18] X. Ke, B. Qian, H. Cao, J. Hu, G. C. Wang, and Z. Q. Mao, Phys. Rev. B **85**, 214404 (2012).

[19] Y. Ando, A. N. Lavrov, and S. Komiya, Phys. Rev. Lett. **90**, 247003 (2003).

[20] A. N. Lavrov, H. J. Kang, Y. Kurita, T. Suzuki, S. Komiya, J. W. Lynn, S. H. Lee, P. C. Dai, and Y. Ando, Phys. Rev. Lett. **92**, 227003 (2004).

[21] J. Wang, J. Deng, X. Liang, G. Gao, T. Ying, S. Tian, H. Lei, Y. Song, X. Chen, J.-g. Guo, and X. Chen, Phys. Rev. Materials **5**, L091401 (2021).

[22] H. Wang, C. Lu, J. Chen, Y. Liu, S. L. Yuan, S.-W. Cheong, S. Dong, and J.-M. Liu, Nat. Commun. **10**, 2280 (2019).

[23] Y. Liu, J. J. Bao, C. Q. Xu, W. H. Jiao, H. Zhang, L. C. Xu, Z. Zhu, H. Y. Yang, Y. Zhou, Z. Ren, P. K. Biswas, S. K. Ghosh, Z. Yang, X. Ke, G. H. Cao, and X. Xu, Phys. Rev. B **104**, 104418 (2021).

[24] T. Krenke, E. Duman, M. Acet, E. F. Wassermann, X. Moya, L. Mañosa, and A. Planes, Nat. Mater. **4**, 450 (2005).

[25] R. Roy Chowdhury, S. Dhara, and B. Bandyopadhyay, Phys. B (Amsterdam, Neth.) **517**, 6 (2017).

[26] Y. Liu, J. Li, J. Tao, Y. Zhu, and C. Petrovic, Sci. Rep. **9**, 13233 (2019).

[27] X. Min, W. L.-Min, P. Rui, G. Q.-Qin, C. Fei, Y. Z.-Rong, Z. Yan, C. S.-Di, X. Miao, L. R.-Hua, S. Ming, C. X.-Hui, Y. W.-Guo, K. Wei, X. B.-Ping, F. D.-Lai, M. Arita, K. Shimada, H. Namatame, M. Taniguchi, M. Matsunami, and S. Kimura, Chin. Phys. Lett. **32**, 027401 (2015).

[28] H. Chen, Q. Niu, and A. H. MacDonald, Phys. Rev. Lett. **112**, 017205 (2014).

[29] J. D. Hoffman, B. J. Kirby, J. Kwon, G. Fabbris, D. Meyers, J. W. Freeland, I. Martin, O. G. Heinonen, P. Steadman, H. Zhou, C. M. Schlepütz, M. P. M. Dean, S. G. E. te Velthuis, J.-M. Zuo, and A. Bhattacharya, Phys. Rev. X **6**, 041038 (2016).

[30] J. D. Hoffman, S. M. Wu, B. J. Kirby, and A. Bhattacharya, Phys. Rev. Applied **9**, 044041 (2018).

[31] S.-H. Yang, Appl. Phys. Lett. **116**, 120502 (2020).

[32] M. Wang, C. Andrews, S. Reimers, O. J. Amin, P. Wadley, R. P. Campion, S. F. Poole, J. Felton, K. W. Edmonds, B. L. Gallagher, A. W. Rushforth, O. Makarovsky, K. Gas, M. Sawicki, D. Kriegner, J. Zubáč, K. Olejník, V. Novák, T. Jungwirth, M. Shahrokhvand *et al.*, Phys. Rev. B **101**, 094429 (2020).

[33] S. P. Bommanaboyena, D. Backes, L. S. I. Veiga, S. S. Dhesi, Y. R. Niu, B. Sarpi, T. Denneulin, A. Kovács, T. Mashoff, O. Gomonay, J. Sinova, K. Everschor-Sitte, D. Schönke, R. M. Reeve, M. Kläui, H.-J. Elmers, and M. Jourdan, Nat. Commun. **12**, 6539 (2021).

[34] S. Yu. Bodnar, Y. Skourski, O. Gomonay, J. Sinova, M. Kläui, and M. Jourdan, Phys. Rev. Applied **14**, 014004 (2020).

[35] X. Marti, I. Fina, C. Frontera, J. Liu, P. Wadley, Q. He, R. J. Paull, J. D. Clarkson, J. Kudrnovský, I. Turek, J. Kuneš, D. Yi, J.-H. Chu, C. T. Nelson, L. You, E. Arenholz, S. Salahuddin, J. Fontcuberta, T. Jungwirth, and R. Ramesh, Nat. Mater. **13**, 367 (2014).

[36] I. Fina, X. Marti, D. Yi, J. Liu, J. H. Chu, C. R.-Serrao, S. Suresha, A. B. Shick, J. Železný, T. JUngwirth, J. Fontcuberta, and R. Ramesh, Nat. Commun. **5**, 4671 (2014).